IEEE Access
Multidisciplinary | Rapid Review | Open Access Journal

Received December 15, 2020, accepted January 4, 2021, date of publication January 8, 2021, date of current version January 22, 2021.

Digital Object Identifier 10.1109/ACCESS.2021.3049914

Optimization and Mechanism of the Wicket Gate Closing Law for High-Head Pumped Storage Power Stations

CHANG LIU, JIANZHONG ZHOU, XINJIE LAI, AND TIANYU ZHANG
School of Civil and Hydraulic Engineering, Huazhong University of Science and Technology, Wuhan 430074, China
Corresponding author: Jianzhong Zhou (jz.zhou@hust.edu.cn)

This work was supported by the National Key Research and Development Program of China under Grant 2016YFC0402205 and Grant 2016YFC0401910.

ABSTRACT The high-head pumped storage power station (PSPS) has complex working conditions and severe transient processes. Under load rejection conditions, the turbine speed and the flow channel pressure will threaten the unit. By adjusting the wicket gate closing law (WGCL), we can effectively alleviate the adverse effects of the transient process. In this study, a full flow channel refined model of a high-head PSPS was constructed, and the influence mechanism of load rejection conditions on key parameters was analyzed by tracking the operating trajectory on the S characteristic curves and simulating the transient flow field inside the pumped turbine by three-dimensional computational fluid dynamics (3D-CFD). Given the contradiction between different parameters in the wicket gate closing process, a third-generation non-dominated genetic algorithm based on reference point selection (NSGA-III) was introduced, and a high-dimensional multi-objective WGCL optimization model was constructed. We compared parameter changes in the two-phase and three-phase WGCL optimized elite solutions and explained the rationality of adopting the three-phase WGCL in high-head PSPSs. By proposing an improved three-phase WGCL, a new scheme—the most suitable WGCL under load rejection—was obtained through precise optimization. The research embodied the excellent effect of the heuristic multi-objective (MO) optimization algorithm based on the Pareto strategy in solving the operation problem of the large fluctuation transient process of hydraulic machinery. It revealed the theoretical basis of engineering adjustment for the safe production and operation of hydropower.

INDEX TERMS Pumped storage power station, one-dimensional method of characteristic, multi-objective wicket gate closing law optimization, non-dominant genetic algorithm based on reference point selection (NSGA-III).

I. INTRODUCTION

Pumped storage power stations (PSPSs) have unique operation modes of peak-valley filling, frequency and phase modulation, and rapid response functions such as spinning reserve, which have become a critical method of green energy production. During PSPS operation, there are often large-scale load changes, such as the full load rejection condition of the turbine and the failure condition of the pump. The pumped turbine with a pressure piping system is affected by the resulting hydraulic transient, and company safety is essential. For instance, the runner speed increases sharply due to the unbalance between the dynamic torque and the resistance torque accompanied by severe pressure pulsation when the unit is in an emergency shutdown for the load rejection, which causes large short-term stress and strain on the unit structure [1].

Under normal circumstances, the wicket gates, which are also called guide vanes, can be closed by the governor in time to reduce the overcurrent flow in the unit to reduce the unit speed. However, closing the wicket gates too quickly will cause greater water hammer pressure in the hydraulic system [2]. The vacuum at the draft tube will drop rapidly due to the rapid decrease in flow rate and even cause water column separation [3]. An improper wicket gate closing law (WGCL) may cause the diversion pipe to rupture. Consequently, the

The associate editor coordinating the review of this manuscript and approving it for publication was Amjad Anvari-Moghaddam.

superposition of the back water hammer will let the unit lift up, producing vibration and noise and causing runaway damage to the unit [4].

There are many ways to analyze the transient flow of turbines during the load rejection process. Several methods are typically used to reflect the key parameters at each moment in the flow field in the flow channel. One is to use the one-dimensional method of characteristics (1D-MOC) [1], [5] and transfer function method (TFM) [6] *et al.* to establish a numerical model of the entire flow channel of the turbine. The 1D transient process analysis simplifies the complicated water diversion system and equipment into simple pipelines and simplified models. The parameter values at the midpoint of the water flow section are measured as values of the node. It is useful for calculating the pressure and other parameter values of equipment or pipelines in large hydropower stations [7], [8].

For addressing the adverse effects of the pumped turbine during the load rejection transient process, the water hammer pressure at the spiral case inlet, the rate increase of the runner speed, and the vacuum at the draft tube outlet were selected as key indicators. Relevant measures were taken to reduce the maximum value of each indicator in this study. However, these key indicators are mutually restrictive. Because of the changes in wicket gate closing time, one indicator tends to deteriorate after the other two indicators are limited. Therefore, the traditional one-phase WGCL can no longer meet the complex load rejection condition.

It is no longer possible in existing power stations to improve the impact of the transition process by changing the shape of the flow channel or constructing safety equipment. Changing the WGCL is critical to weighing the contradiction between the three sets of key indicators. An appropriate WGCL can simultaneously optimize different indicators. The influence of the closing process of the movable wicket gates on the key indicators and the transient change in the flow channel have been recently analyzed [9]–[11].

Traditional nonlinear WGCLs include the ladderlike pattern [9], two-phase [12] strategy, and three-phase [13] strategy, which involve the determination of the coordinates of different inflection points on the wicket gate closing curve. Simultaneously, the WGCL optimization problem has multiple objective functions and constraints, referred to as a multi-objective WGCL (MOWGCL) problem. Previous researchers have applied the heuristic optimization algorithms to the flow channel design and parameter optimization of hydraulic equipment [14]–[16], and several optimization studies have examined the MOWGCL problem [17], [18]. However, previous studies usually converted the multi-objective optimization problem (MOOP) into one or two objective functions by setting weighting coefficients, which has intense subjectivity in optimization.

The heuristic algorithm based on Pareto theory has significant advantages for solving MOOP [20]. In 2014, Deb *et al.* [21], [22] proposed the third-generation non-dominated sorting genetic algorithm (NSGA-III). It is a new type of multi-objective genetic algorithm that addresses the defects of the second-generation non-dominated sorting genetic algorithm (NSGA-II) [23]. It has numerous advantages, such as fast calculation speed, strong robustness, and uniform distribution of non-inferior optimal solutions. Simultaneous-ly, the diversity and convergence of Pareto solution set are improved through the setting of reference points [24]. Recent studies have further improved the algorithm [25], [26]. At present, many studies have applied NSGA-III to production practice to solve engineering problems involving multiple parameters and multiple objectives [27]–[29].

This study combined the performance analysis of the transient process and the multi-objective (MO) optimization algorithm, and the WGCL under full load rejection conditions was studied and analyzed. We have established a one-dimensional (1D) refined model of the entire flow path in this PSPS, calculated the change law for the key indicators, and analyzed the operating trajectory of the unit in the S characteristic region and the 3D eddy current vibration under load rejection conditions. Based on the analysis results, NSGA-III was used to optimize the WGCL accurately. The performance change curves of different forms of WGCL were explored, and the optimal optimization strategy was obtained through multi-angle comprehensive analysis results. The research results contri-bute to exploring rational and easy-to-operate WGCLs in the hydraulic transient process and providing references for the safe operation and management of hydropower stations.

II. SIMULATION MODEL

A. RESEARCH OBJECT

The high-head PSPS in Jiangxi Province, China, is equipped with four pumped turbine units with a rated power of 306.1 MW, and every two units is installed under the same pipeline system. This study conducted 1D-MOC modeling and simulation on a single device of a single pipeline.

The relevant parameters of the power station turbine are depicted in Table 1. According to the parameters, the pumped turbine has a high specific speed and high head. According to the hydraulic model test report at design time, the equipment has an apparent S-shaped area during the transient load rejection process. It will produce greater flow and torque fluctuations [30].

Fig. 1 illustrates the general schematic diagram of the research model. MOC was used to determine the four pipeline sections from the casing inlet of the upstream reservoir and the draft tube outlet to the downstream reservoir. Other equipments were modeled using 1D methods.

B. 1D-MOC MODEL

By using 1D-MOC to build the numerical model of the unsteady flow in a pressure pipeline, the unsteady flow equation and continuity equation in the pressure pipeline can be described as [31]:

$$\frac{\partial Q}{\partial t} + gF\frac{\partial H}{\partial L} + \frac{f}{2DF}Q|Q| = 0 \tag{1}$$

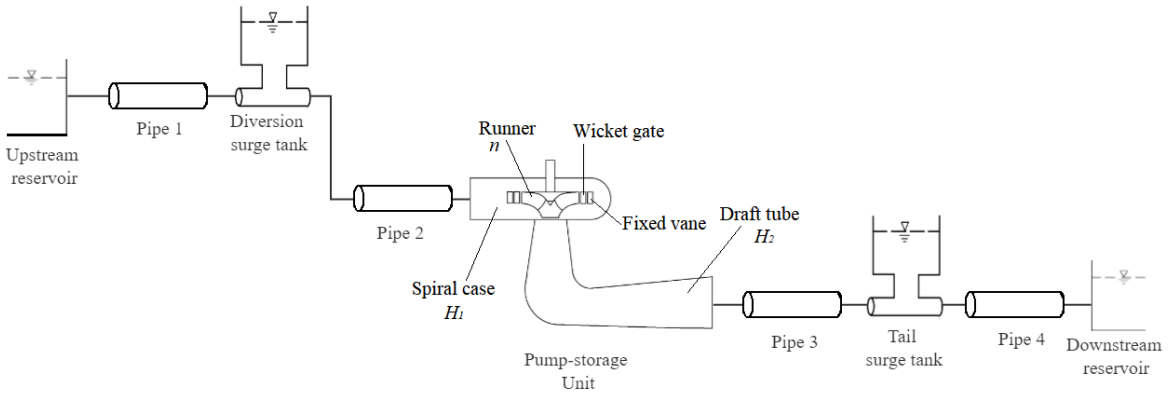

FIGURE 1. 1D calculation model of PSPS.

TABLE 1. Equipment parameters of a single pumped turbine.

Project	Symbol	Value
Rated Power	P	306.1MW
Specific speed	n_r	35.15
Rated speed	n	500r/min
Draft head	H_s	-70.0m
Rated head	H	540.0m
Rated flow	Q	62.09m^3/s

$$c^2\frac{\partial Q}{\partial L}+gF\frac{\partial H}{\partial t}=0 \tag{2}$$

The characteristic equation of the overcurrent system is:

$$Q_P = C_p - C_a H_P \tag{3}$$

$$Q_P = C_n + C_a H_P \tag{4}$$

among them

$$C_p = Q_A + C_a H_A - C_f Q_A |Q_A| \tag{5}$$

$$C_n = Q_B - C_a H_B - C_f Q_B |Q_B| \tag{6}$$

$$C_a = gF/c \tag{7}$$

$$C_f = f\Delta t/2DF \tag{8}$$

Eqs. (3) and (4), respectively, represent the MOC equations along $+c$ and $-c$ in the transmission direction of the water hammer wave in the same or opposite direction of the water flow. Q_i and H_i respectively represent the flow and water head at the corresponding node of the unit pipeline. The subscript P represents the intersection of the positive and negative characteristic lines between the two points A and B, and Δt is the simulation time step. Based on Eqs. (3) and (4), combined with the elastic water hammer effect, 1D-MOC equations were established for each hydraulic unit, upper and lower reservoirs, and surge tanks of the PSPS overwater system, and the flow and head changes in each node of the pipeline were iteratively solved.

The complete characteristic curve interpolation model was used to simulate the changes in the parameters of the pumped turbine under the transient state, and the speed curves of the runner were applied to the 3D-CFD as boundary conditions. Simultaneously, the pumped turbine is relatively distorted at the S characteristic curve. Therefore, according to the Refs. [32], [33], the improved Suter transformation method (ISTM) was used to eliminate undesirable phenomena such as the intersection and overlap of the original S-curve. With the wicket gate opening α as an independent variable, the corresponding flow characteristic curve $Q_{11} \sim n_{11}$ and torque characteristic curve $M_{11} \sim n_{11}$ were established. The key parameters of the pumped turbine were calculated according to Eq. (10).

$$\begin{cases} Q_{11} = Q_{11}(\alpha, n_{11}) \\ M_{11} = M_{11}(\alpha, n_{11}) \end{cases} \tag{9}$$

$$\begin{cases} n = n_{11}\sqrt{H}/D_1 \\ Q_t = Q_{11}D_1^2\sqrt{H} \\ M_t = M_{11}D_1^3 H \end{cases} \tag{10}$$

The generator motor was described by a first-order model, and its dynamic equation is:

$$T_a\frac{dn}{dt} + e_n(n - n_0) = m_t - m_e \tag{11}$$

where T_a represents the inertia time constant of the generator, which represents the time required for the rotor to accelerate from a standstill to the rated speed when the prime mover applies a rated torque ($m_t = 1$) when it is in the no-load state ($m_e = 0$). n is the relative speed, n_0 is the relative speed of the previous time step, e_n is the unit self-adjustment coefficient, $m_t = (M_t - M_{t0})/M_r$ and $m_e = (M_e - M_{e0})/M_r$, respectively, represent the relative deviation of the prime mover main torque and the load resistance torque.

The wicket-gate-closing system model was simulated by the TFM of the speed control system and considered the nonlinearity of the hydraulic system. The upstream and downstream surge tanks also used linear dynamic equations for first-order modeling.

C. MODEL VERIFICATION CALCULATION

The single-tube and single-unit of the PSPS were calculated under 100% and 75% load rejection conditions, and the processes were based on the designed one-stage WGCL. We compared the difference between the model simulation

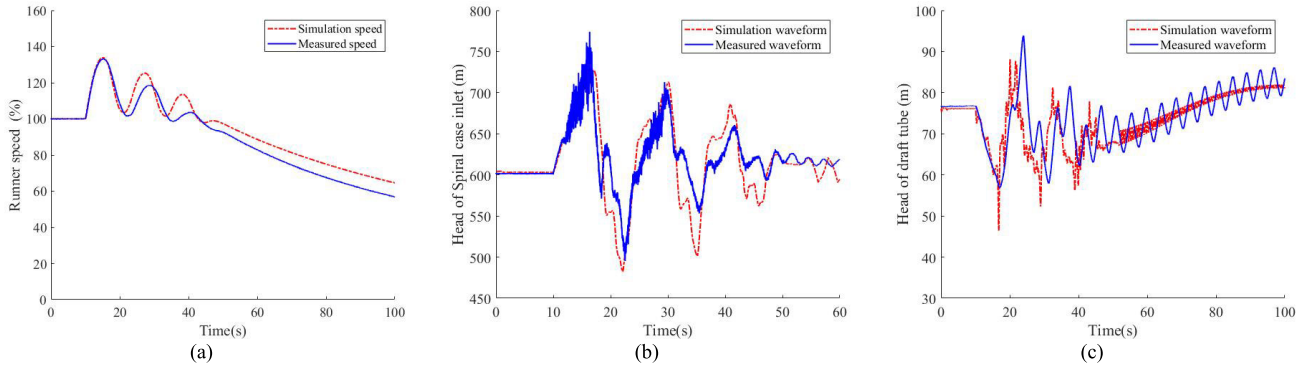

FIGURE 2. Comparison of simulation curve of 1D-MOC model with measured curve: (a) Comparison of the runner speed rate change (b) Comparison of the spiral case inlet pressure (c) Comparison of the draft tube outlet pressure.

results and the measured parameters and analyzed whether the test results fit. Fig. 2 is a comparison diagram of simulated and real-world parameters under 100% load rejection. Based on the experimental results, the correspond-ing performance indicators were calculated and compared with the real-world data to obtain the data depicted in Table 3. Under three load rejection conditions with different initial conditions, the variation curve of each parameter and the real-world data were within the allowable error range, confirming that the 1D-MOC model has high reliability.

III. IMPACT MECHANISM ANALYSIS OF KEY INDICATORS

A. ANALYSIS OF CHARACTERISTIC CURVE

In the high-head pumped turbine, the load rejection condition is located in the S-region of the complete characteristic curve. The running trajectory crosses a runaway curve frequently, which is likely to cause damage to the unit. Figs. 3 and 4, respectively, illustrate the operation trajectory in the S-region and the key indicator change curves of the pumped turbine under load rejection conditions. The operation trajectory starts from Point 1 and first moves down the curve until it reaches Point 5. On the way, it reaches singular points at Points 2 and 4 and intersects the runaway curve at Point 3 (the runaway point). At this time, the speed reaches the maximum or minimum.

We analyzed the impact of these points on the operating conditions of the pumped turbine. Based on Eq. 12, the rate of change in the water hammer pressure at the spiral case inlet over time can be obtained by the following equation[9]:

$$\frac{\Delta h}{\Delta t} = \frac{2h^{3/2}}{n'_{11} - Q'_{11}/a}\left(\frac{1 - 1/h}{aT_w} + \frac{M'_{11}}{T_a}\right) \tag{12}$$

where $a = \mathrm{d}Q'_{11}/\mathrm{d}n'_{11}$ is the slope of any point on operation trajectory.

After combining Eq. 12 and the indicator change curve obtained by simulation calculation, the hydraulic character-istics change law of the pumped turbine under load rejection conditions can be obtained. The result was consis-tent with the derived formula.

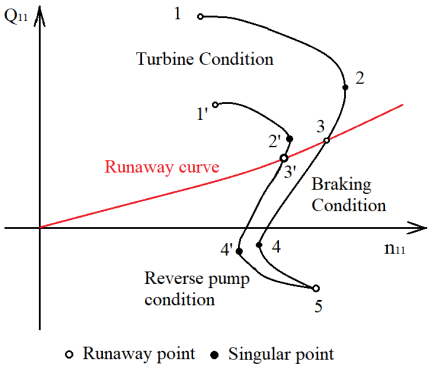

FIGURE 3. Operation trajectory of S-characteristic curve under load rejection condition.

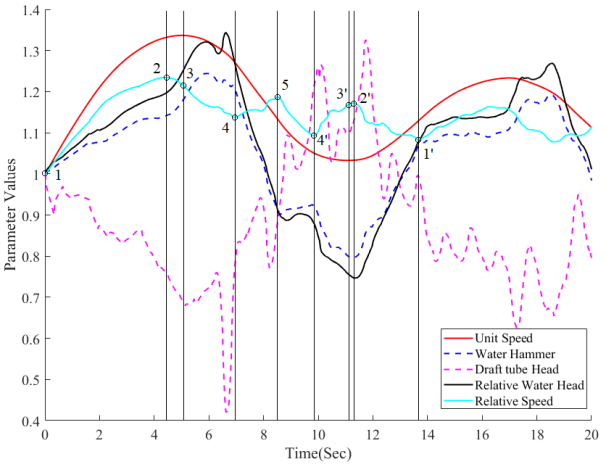

FIGURE 4. Comparison curve of dimensionless unit speed and key indicators quantity under load rejection conditions.

1) POINT 1 TO 2

Because the unit suddenly loses its full load, the dynamic torque is greater than the resistance torque. Moreover, the resultant torque is positive, causing the runner to suddenly increase in speed after load rejection and the wicket gates to start closing. At this time, n'_{11} gradually rises and reaches a maximum value at Point 2, and the rotation speed n of the

TABLE 2. Comparison of various parameters of the three sets of load rejection experiments.

Experimental conditions	Upper reservoir level (m)	Lower reservoir level (m)	WGCLs	Parameters	Actual measurement data	Simulation data	Relative error
100% load rejection	730.4	168.5	42.00-0-0.97	Maximum increase value of runner speed (%)	1.3336	1.3368	0.24%
				Minimum head at the casing inlet (m)	491.40	478.32	2.66%
				Maximum head at the casing inlet (m)	775.90	739.66	4.67%
				Minimum head at the draft tube outlet (m)	56.88	47.27	16.89%
75% load rejection	729.3	169.4	34.89-0-0.78	Maximum head at the draft tube outlet (m)	93.88	88.85	5.36%
				Maximum increase value of runner speed (%)	1.2509	1.2838	2.63%
				Minimum head at the casing inlet (m)	521.20	498.25	4.40%
				Maximum head at the casing inlet (m)	747.90	718.36	3.95%
				Minimum head at the draft tube outlet (m)	48.84	42.88	12.20%
				Maximum head at the draft tube outlet (m)	100.80	96.70	4.07%

runner also rises correspondingly. The spiral case water hammer head H_1 and the relative head h have the same changing trends, and the draft tube head H_2 and h have opposite trends. The water hammer pressure continues to rise at this stage, and the draft tube pressure continues to drop.

2) POINT 2 TO 3

As the wicket gates continue to close, after experiencing Singular Point 2, n'_{11} begins to fall. n and H_1 continue to rise, and H_2 continues to fall, so h also continues to rise. The total torque of the turbine is 0, and the runner enters the runaway speed at $t = 4.4$ s. The corresponding point on the S-curve is Point 3. Here is the dividing point of the pumped turbine from the turbine operating condition to the braking condition. It is also a dangerous point.

3) POINT 3 TO 4

After entering the braking region, the wicket gates continue to close, n'_{11} continues to fall to the minimum, and h reaches the maximum point close to Point 4. Because the resistance torque caused by the decrease in flow is greater than the dynamic torque, n begins to decrease. The first-phase water hammer wave is transmitted to the spiral case inlet, and the maximum value of H_1 appears at $t = 5.8$ s immediately after Point 3. The water hammer wave then rebounds, a longer vortex appears at the pumped turbine draft tube, and H_2 reaches the minimum. Considering H_1 and H_2 comprehensively, the changing law of h is not apparent. In this process, the operation trajectory changes from the braking condition to the reverse pump condition.

4) POINT 4 TO 5

In the reverse pump condition, the first-phase water hammer wave is transmitted in the reverse direction, and the unit flow rate Q'_{11} is negative. h begins to drop sharply, and n slowly decreases, so n'_{11} begins to rise. In this process, the primary manifestation is that H_1 decreases rapidly, and the change in H_2 is not apparent.

5) POINT 5 TO 4′

The operation trajectory starts to slide upwards after reaching Point 5; ideally, it will return to Point 1, but due to hydraulic loss, after reaching the runaway Point 5, the running trajectory starts to shift to the left and n'_{11} decreases to reach Point 4'. n continues to fall, the changes in H_1 and H_2 are uncertain, the change in h is uncertain, and H_2 is generally in the rising stage.

6) POINT 4′ TO 2′

In this process, n'_{11} moves from the minimum point to the maximum point, and h is continuously declining. n reaches the minimum value at $t = 11.1$ s, for the runaway Point 3' in the S-curve. H_1 decreases gradually, and H_2 changes uncer-tainly.

7) POINT 2′ TO 1′

In this stage, the second phase water hammer begins to pass forward, n'_{11} decreases, and h begins to rise. The water hammer drives the dynamic torque to increase, n begins to increase, H_1 rises sharply, and H_2 decreases. The subsequent hydraulic transient process continues the law of change in step 1, but with the hydraulic loss, the extremums of rotation speed, water hammer pressure, and draft tube pressure cannot exceed these in the first phase process.

B. INTERNAL FLOW FIELD ANALYSIS

We further demonstrate the change characteristics of the load rejection conditions of the pumped turbine using 3D computational fluid dynamics (3D-CFD) and dynamic mesh technology to analyze the internal transient flow field

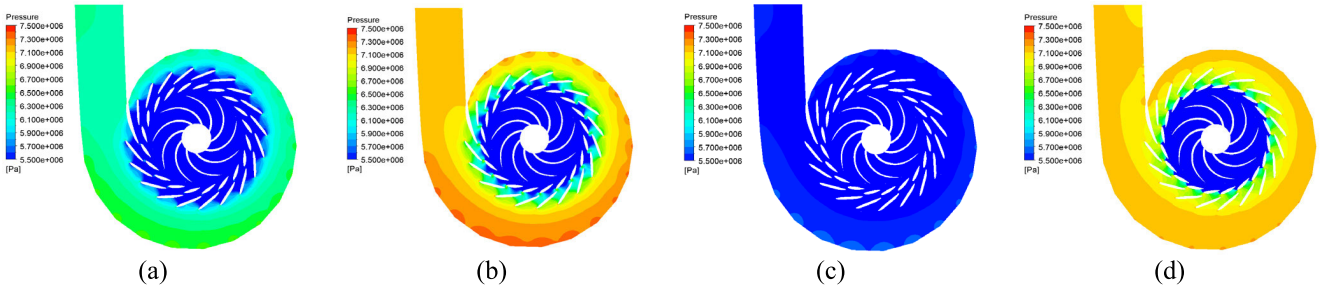

FIGURE 5. Water hammer pressure distribution of the spiral case under load rejection condition (a) t = 2s; (b) t = 7s; (c) t = 11s; (d) t = 19s.

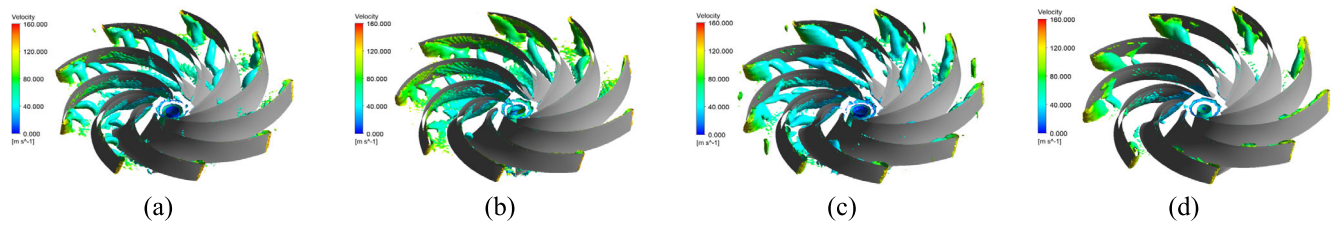

FIGURE 6. The distribution of eddy currents inside runner blades under load rejection conditions (a) t = 2s; (b) t = 7s; (c) t = 12s; (d) t = 21s.

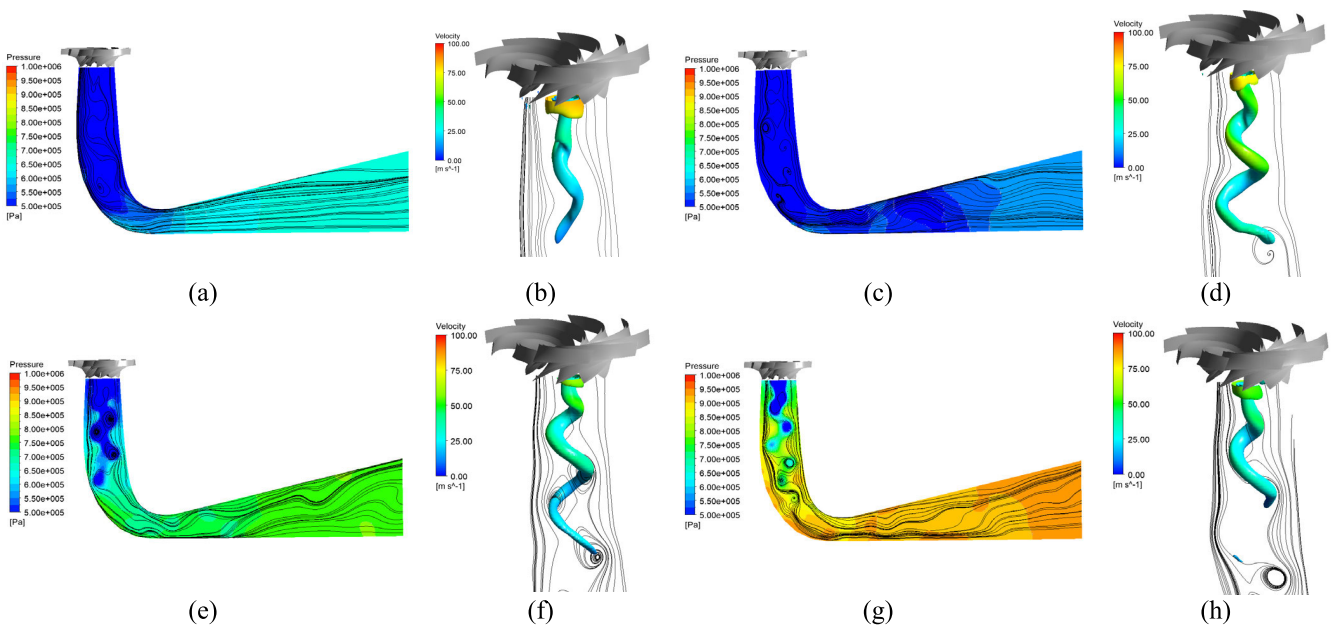

FIGURE 7. Draft tube pressure and vortex distribution under load rejection conditions. Draft tube pressure and streamline: (a) t = 3s; (c) t = 7s; (e) t = 11s; (g) t = 14s;. Draft tube vortex and streamline: (b) t = 3s; (d) t = 7s; (f) t = 11s; (h) t = 14s.

during the wicket gate closing. Fig. 5 illustrates the pressure distribution of the horizontal section on the spiral case at $t = 2, 7, 11, 19$s. We can observe the pressure distribution of the flow field caused by the first and second phase water hammer. The inertial centrifugal force of the water flow produced a relatively large pressure on the outer wall of the spiral case. Simultaneously, the pressure difference between the fixed vanes and the wicket gates was large, which readily generates the Karman vortex street and induces unit vibration.

Fig. 6 illustrates the vortexes inside the runner blade at $t = 2, 7, 12, 21$s. After the load rejection, impact vortexes at the inlet side of the runner blades were caused by the drastic change in the internal flow of the pumped turbine. The reduction of flow caused channel vortexes at the back of the blades. As the runner's rotating speed increases, the impact vortexes and channel vortexes gradually develop and connect to form a larger vortex region, causing violent vibration and even cavitation.

Fig. 7 illustrates the pressure distribution and vortex strip of the draft tube at $t = 3, 7, 11, 14$s under load rejection. After the wicket gates were closed, the draft tube pressure first decreased and then increased. The vortex strip began to develop and grow with runner wake disturbance during pressure reduction. Hitting of the draft tube outer wall by

the vortex strip can cause vibration and safety accidents. Along with the pressure rises, the vortex strip dissipated, and cavitation and cavitation were likely to occur, which can damage the unit.

Therefore, the key indicators of unit are closely related to the flow field changes inside the pumped turbine. By optimizing the performance indicators during load rejection conditions, the water hammer fluctuation and cavitation vibration of the pumped turbine can be solved. Consequently, the level at which the unit can be safely operated can be improved.

C. WGCLs

The rotation of wicket gates of the pumped turbine is driven by the governor. Commonly used WGCLs include one-phase, ladderlike pattern, two-phase and three-phase. As the most basic WGCL, the one-phase scheme has the advantages of simple operation and easy implementation. It only must optimize its closing time, but its optimized space is small and cannot meet the safety requirements of complex working conditions. A ladderlike pattern WGCL has been used in some PSPSs in production, such as the Heimifeng and Xianyou power stations in China [34]. It can effectively control the increase in water hammer pressure but cannot suppress the increase in speed. At present, the primary method for solving the MOWGCL problem is to use two-phase and three-phase WGCL.

The two-phase WGCL divides the closing of the wicket gates from fully open to fully closed into two parts. In each closing period, straight-line sections with different slopes are used. The two-phase WGCL is divided into two forms: fast-first-and-then-slow and slow-first-and-then-fast, as depicted in Fig. 8. For conventional pumped turbines, there is a theoretical basis for adopting the WGCL of fast-first-and-then-slow. At the beginning of load rejection, the closing speed of the wicket gates is fast, so that the trajectory from 1 to 3 in Fig. 3 moves to the left, which is beneficial for reducing the increase in speed. When the pressure rise value reaches the specified value, the wicket gates start to close slowly, such that the subsequent water hammer pressure rise rate will not be higher than that at the turning point. Properly selecting the turning point position and the closing speed of the first and second phases can reduce the water hammer pressure and speed rise rate.

The closing steps of the three-phase WGCL are as follows. When the unit changes working conditions, the wicket gates close quickly in the first phase. There are three forms in the second phase: reopened, delayed, and closed. The wicket gates are turned off entirely in the third phase, as depicted in Fig. 9. This WGCL has a flexible adjustment method and can effectively solve the contradiction between different key indicators. However, choosing the turning point time and the opening is challenging.

IV. OPTIMIZATION OF WGCL

The WGCL of the pumped turbine is a high-dimensional multi-objective optimization problem (MOOP). This research

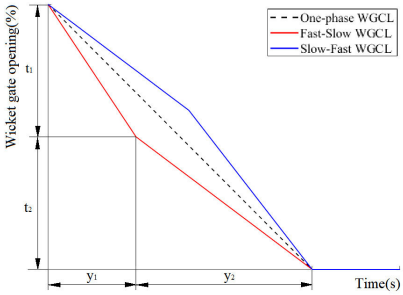

FIGURE 8. 1-phase and 2-phase WGCLs.

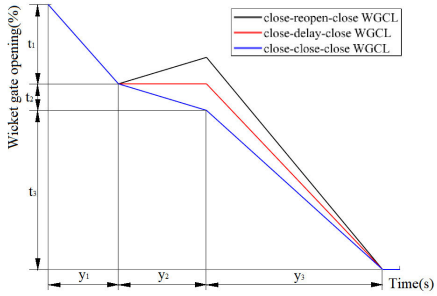

FIGURE 9. 3-phase WGCLs.

studied a third-generation non-dominant genetic algorithm (NSGA-III) based on the selection of reference points, and the WGCL in load rejection conditions is optimized. We selected the speed increase rate, the water hammer pressure at the casing inlet, and the water hammer pressure at the draft tube outlet under the 100% load rejection of the pumped turbine as the high-dimensional multi-objective function, and we set the relevant constraints. After 100 iterations of analysis, the curve of the key parameters of the pumped turbine transient process was obtained. The calculation example reflected the excellent role of NSGH-III in optimal decision-making and combined engineering to satisfy comprehensive countermeasure decision-making.

A. THEORIES OF NSGA-III

A non-dominated sorting genetic algorithm (NSGA) is a genetic algorithm based on Pareto optimal solution set, which solves different solutions by judging the dominance relationship. The population of each generation is stratified by setting the corresponding virtual fitness value, and the resulting solution set cannot further optimize one or more objectives without restraining other objectives [35-38].

The improved algorithm, NSGA with elite strategy (NSGA-II), uses a fast non-dominated sorting method, which reduces computational complexity. NSGA-III has further improved the previous algorithm. NSGA-III uses a set of evenly distributed reference points niche technology to maintain population diversity.

The following are the primary selection steps of NSGA-III.

1) DIVIDE THE NON-DOMINATED LAYER

Assuming that P_t is the parent of the tth generation and the number of individuals is N, the offspring Q_t is generated through crossover and mutation operations, and the number of individuals is also N. We combine the offspring and the parents into a new population $R_t = P_t \cup Q_t$ with $2N$ individuals and select N individuals by determining Pareto dominance. We compare all individuals in R_t with other individuals in their dominance relationship, perform a non-dominated ranking, and then divide them into multiple non-dominated layers ($F_1, F_2, \ldots$). F_1 constructs a new population S_t. If the number of individuals in the population satisfies $|S_t| < N$, the next layer F_2 is added to the middle S_t, and so on, until $|S_t| = N$ is satisfied. If $|S_t| = N$, then S_t is the new generation of population $P_{t+1} = S_t$. If $|S_t| > N$, and the non-dominated layer just added to S_t at this time is F_l, layer 1 is only partially accepted. Part of the next-generation solution is $P_{t+1} = \cup_{i=1}^{l-1} F_i$, and the remaining K solutions ($K = N - |P_{t+1}$) are selected from F_l, as depicted in Fig. 10.

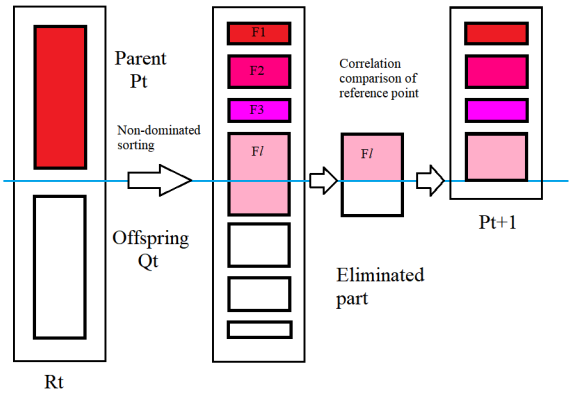

FIGURE 10. Elite strategy in NSGA-III.

2) SELECT OPERATION

The reference point on the hyperplane must be determined. NSGA-III usually uses Das and Dennis's method (DDM) [39] to generate a set of structured reference points to ensure the diversity of solutions. If the number of optimization targets is M, an (M-1)-dimensional hyperplane must be generated so that the reference points are distributed on the hyperplane. Based on the division number H of the optimization target, the number of reference points is determined [40].

$$P = \begin{pmatrix} M + H - 1 \\ H \end{pmatrix} \tag{13}$$

For ensuring that the measurement scale of each objective function of the individuals in the solution set is fair, it is necessary to perform adaptive normalization processing on the population individuals in advance. First, set an M-dimensional ideal point $\bar{z} = \left(z_1^{\min}, z_2^{\min}, \ldots, z_M^{\min}\right)$, where $z_i^{\min}, i = 1, 2, \ldots, M$ is the minimum value of the population S_t in $\cup_{\tau=0}^{t} S_\tau$. We transform the objective function $f_i(x), i = 1, 2, \ldots, M$ through this ideal point, so that $f_i'(x) = f_i(x) - z_i^{\min}$. Second, find the extreme point corresponding to each coordinate axis, through which we can construct a hyperplane. Finally, using the pitch between the hyperplane and the coordinate axis, the objective function value can be self-adaptively normalized. For the ith conversion target f_i', an additional target vector $z^{i,\max}$ is generated. These M additional target vectors form an M-dimensional linear hyperplane.

After finding the intercept $a_i, i = 1, \cdots, M$, the objective function can be normalized to:

$$\begin{aligned} f_i^n(x) &= f_i'(x) / \left(a_i - z_i^{\min}\right) \\ &= \left(f_i'(x) - z_i^{\min}\right) / \left(a_i - z_i^{\min}\right), \quad i = 1, 2 \ldots, M \end{aligned} \tag{14}$$

After adaptively normalizing each objective function corresponding to the population S_t individual, in the M-dimensional space, the coordinate origin is connected with each reference point to generate a reference line corresponding to each point. We then associate each individual in the population S_t with its nearest reference line and calculate the vertical distance between the individual and the reference line, such that the population individual is associated with the reference point.

We improve the algorithm's convergence with the Niche-Preservation method to select the remaining K solutions to enter the next population. The selection mechanism is proposed in [36], [38].

3) CREATE OFFSPRING POPULATION BY GENETIC OPERATOR

After forming a new generation of population P_{t+1}, we continue to use conventional crossover and mutation operators to construct progeny population Q_{t+1} to determine whether the number of iterations has been reached, and terminate the calculation if it has. Otherwise, the iterative calculation will start from step 1. In NSGA-III, by associating each individual of the population with its reference point, an elite strategy selection can be used. Accordingly, and the diversity of the understanding set is maintained with fast calculation.

The process chart for optimizing WGCL through NSGA-III is depicted in Fig. 11.

B. NSGA-III TO OPTIMIZE WGCL

Based on PSPS operation, this study selected two-phase and three-phase broken-line WGCLs for optimization.

1) OPTIMIZATION VARIABLES

For the two-phase WGCLs, the wicket gate opening y_1 at the turning point and the closing time t_1 and t_2 before and after the turning point were selected as the variables to form the vector $X = [t_1, t_2, y_1]$ to be optimized. During operation, the initial wicket gate opening is 0.97. After the turning point, the wicket gates were closed completely. Similarly, for the three-phase WGCLs, the vector to be optimized was $X = [t_1, t_2, t_3, y_1, y_2]$. The closing speed of the wicket gates

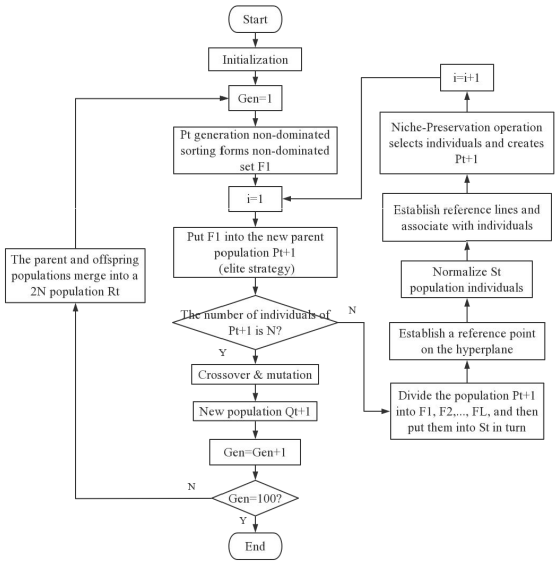

FIGURE 11. NSGA-III algorithm process chart.

changed at the first turning point and closed, and the wicket gates were closed completely after the second turning point, i.e., $y_3 = 0.97 - y_1 - y_2$.

According to the requirements of the load-rejection condition-adjustment guarantee calculation in the pumped turbine, we selected runner rotation speed increase n, water hammer pressure of the spiral case inlet H_1, and draft tube outlet pressure H_2 as key evaluation indicators. Accordingly, we established objective functions reflecting these three indicators:

$$\min f_n = \frac{\max(n_i) - n_r}{n_r}, \quad i = 1, \cdots, N \tag{15}$$

$$\min f_{H_1} = \frac{\max(H_{1,i}) - H_{1,r}}{H_{1,r}}, \quad i = 1, \cdots, N \tag{16}$$

$$\min f_{H_2} = -\frac{\min(H_{2,i}) - H_{2,r}}{H_{2,r}}, \quad i = 1, \cdots, N \tag{17}$$

2) CONSTRAINT CONDITIONS

We establish multiple constraints for the MOWGCL optimization problem.

a: TIME OF WICKET GATE CLOSING

$$\begin{cases} 0 < t_i < T, i = 1, \cdots, p \\ 0 < \sum_{i=1}^{p} t_i < T \end{cases} \tag{18}$$

where t_i is the closing time of the ith segment wicket gate, p is the total number of phases of WGCL, and T is the maximum limit time, selected here as $T = 80$s.

b: AMPLITUDE OF WICKET GATE CLOSING

The amplitude of any phase of the wicket gate closing cannot exceed the total opening of 0.97, i.e., $0 < y_i < 0.97$, $i = 1, \cdots, p$. In the three-phase WGCLs, if the second phase operation mode is reverse opening, i.e., $y_2 < 0$, then $y_1 > -y_2$ is required.

c: SPEED OF WICKET GATE CLOSING

During the closing process, the speed of the wicket gate closing cannot exceed the maximum speed enabled by the servomotor, i.e., the absolute value of the slope of any section of the wicket gate closing curve cannot exceed $k_{\max} = 1.12/27$.

$$k_i = \left| \frac{y_i}{t_i} \right| \le k_{\max}, \quad i = 1, \cdots, p \tag{19}$$

d: RISE RATE OF RUNNER SPEED

$$f_n \le c_n \tag{20}$$

where f_n is the speed increase rate of the first unit, and c_n is the constraint limit constant of the speed increase rate.

After establishing the 1D model of the above-mentioned pumped storage unit as the optimization algorithm's evaluation function, the parameter settings of NSGA-III are obtained as presented in Table 3. After setting the parameters, we run the optimization program to obtain the final optimal Pareto solution.

TABLE 3. NSGA-III algorithm parameter settings.

Parameters	Values	Parameters	Values
The maximum number of iterations *MaxIter*	100	Percentage of Crossover *pCrossover*	0.5
Population size *nPop*	30	Percentage of Mutation *pMutation*	0.5
Number of reference points	10	Mutation rate *mu*	0.02

C. ROBUSTNESS TEST OF NSGA-III

Load rejection conditions under three different initial conditions (design flood level, normal storage level, and dead water level) were selected, and three-phase WGCLs were used for optimization calculations. The results verified the robustness of NSGA-III to solve the MOWGCL problem. The initial conditions are depicted in Table 4.

TABLE 4. Three initial conditions.

Relevant parameters	Design flood level	Normal storage level	Dead water level
Upstream reservoir level (m)	734.78	730.40	716.00
Downstream reservoir level (m)	183.29	168.50	163.00
Initial flow (m^3/s)	61.16	62.09	60.85

Based on the optimized WGCLs under different initial conditions, the optimal elite strategy was selected. Different performance indicators were calculated and compared with the performance indicators of the initial one-phase WGCLs. The results are depicted in Table 5.

TABLE 5. Performance changes of optimized solutions under different initial conditions.

Initial conditions	Initial 1-phase WGCLs	Optimized 3-phase WGCLs	Key indicators	Initial values	Optimized values	Change rates (%)
Design flood level	42-97	2.75-32.11-33.76-11.1-23.8	f_n	0.3268	0.3187	-2.48
			f_{H1}	0.2266	0.2132	-5.91
			f_{H2}	0.4334	0.4180	-3.55
Normal storage level	42-97	2.68-20.60-27.58-11.1-4.8	f_n	0.3390	0.3303	-2.57
			f_{H1}	0.2326	0.2107	-9.42
			f_{H2}	0.5295	0.5050	-4.63
Dead water level	42-97	2.79-35.88-14.79-10.5-31.1	f_n	0.3285	0.3214	-2.17
			f_{H1}	0.2347	0.2214	-5.67
			f_{H2}	0.5610	0.5261	-6.22

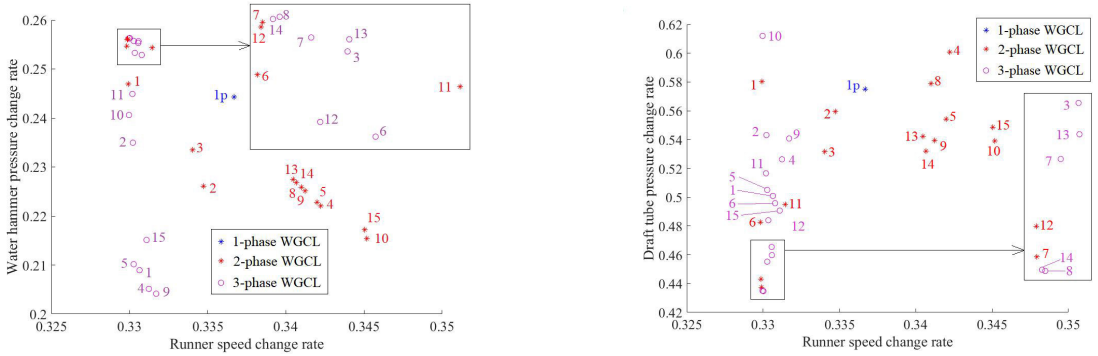

(a) (b)

FIGURE 12. Elite solutions of different forms of WGCL (a) Change rate distribution of speed and water hammer pressure; (b) Change rate distribution of speed and draft tube pressure.

TABLE 6. 1-phase and 2-phase WGCL optimization schemes and performance parameters.

Elite solutions		t_1(s)	t_2(s)	y_1(%)	f_n	f_{H1}	f_{H2}
1-phase	1p	35.0	0	97.0	0.3367	0.2443	0.5752
	1	3.16	41.84	13.1	0.3299	0.2469	0.5802
	2	**1.08**	**47.49**	**4.5**	**0.3347**	**0.2261**	**0.5595**
	3	**2.32**	**42.63**	**7.9**	**0.3340**	**0.2335**	**0.5316**
	4	6.08	39.48	10.4	0.3422	0.2221	0.6009
	5	7.56	30.40	12.3	0.3419	0.2228	0.5544
	6	**4.23**	**41.88**	**17.6**	**0.3298**	**0.2546**	**0.4826**
	7	5.86	25.94	24.3	0.3299	0.2562	0.4374
2-phase	8	14.93	25.94	29.2	0.3410	0.2258	0.5790
	9	7.46	30.57	14.2	0.3412	0.2250	0.5394
	10	9.36	28.30	10.3	0.3452	0.2154	0.5390
	11	2.17	28.21	8.5	0.3315	0.2543	0.4951
	12	**4.47**	**28.21**	**18.5**	**0.3299**	**0.2560**	**0.4430**
	13	6.11	39.62	12.6	0.3405	0.2275	0.5423
	14	14.01	27.09	28.3	0.3407	0.2269	0.5319
	15	14.93	24.07	16.9	0.3450	0.2172	0.5485

After comparing the change rates of key indicators under different initial conditions, regardless of which initial conditions are optimized, improved WGCLs can be obtained. The change rates of the optimized solution indicators were all in a relatively similar range, and the broken laws of the three groups of optimization schemes were roughly equivalent. Consequently, our algorithm is highly robust.

V. RESULT ANALYSIS

A. COMPARISON OF DIFFERENT FORMS OF WGCL

Many studies have been conducted to optimize the one-phase WGCLs of this PSPS, with a total closing time of $t_1 = 35$s. After comparison, the performance indicators of the optimization results exceed the design WGCL in all aspects. With NSGA-III to optimize the two-phase and three-phase WGCLs, after 100 iterations, the 30 individuals in the population were sorted non-dominantly. The first 15 solutions with the least reference points were selected as the elite solutions. The comparison of one-phase and two-phase optimization results is depicted in Table 6, and the comparison of three-phase optimization results is depicted in Table 7. With the three performance parameters as the benchmark, the obtained elite solution set is depicted in Fig. 12.

We establish the following definition. Suppose all performance indicators of Solution A outperform those of Solution B. In that case, Solution A is completely non-dominated by B.

TABLE 7. 3-phase WGCL optimization scheme and performance parameters.

Elite solutions	t_1(s)	t_2(s)	t_3(s)	y_1(%)	y_2(%)	f_n	f_{H1}	f_{H2}
1	**2.59**	**19.07**	**30.59**	**10.6**	**5.0**	**0.3306**	**0.2089**	**0.5009**
2	3.41	19.36	34.40	13.9	14.1	0.3302	0.2350	0.5432
3	2.37	17.71	31.44	9.6	58.3	0.3306	0.2553	0.4654
4	**2.47**	**20.94**	**32.75**	**10.0**	**2.5**	**0.3312**	**0.2051**	**0.5263**
5	**2.68**	**20.60**	**27.58**	**11.1**	**4.8**	**0.3302**	**0.2102**	**0.5050**
6	2.47	19.29	27.18	10.0	57.3	0.3308	0.2529	0.4959
7	2.45	18.78	31.77	10.1	63.9	0.3303	0.2557	0.4552
8	5.80	18.81	18.36	23.9	39.0	0.3300	0.2563	0.4348
9	2.32	17.10	28.65	9.4	3.4	0.3317	0.2041	0.5407
10	3.54	18.20	34.29	14.6	17.0	0.3299	0.2406	0.6120
11	4.39	11.42	34.29	17.9	-5.1	0.3302	0.2449	0.5166
12	2.45	19.25	28.43	10.1	58.1	0.3303	0.2533	0.4840
13	2.41	17.97	31.40	9.8	60.7	0.3306	0.2557	0.4597
14	**5.77**	**26.16**	**13.20**	**23.8**	**58.3**	**0.3299**	**0.2562**	**0.4350**
15	2.44	15.90	34.29	9.9	13.5	0.3311	0.2151	0.4907

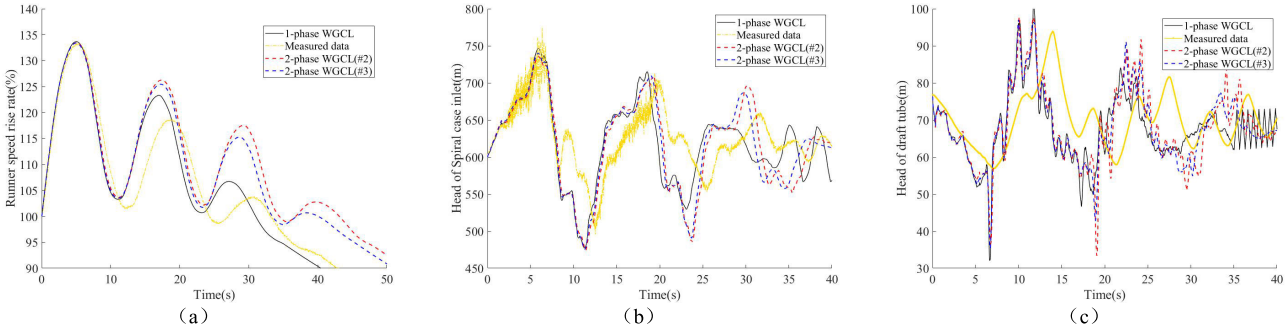

FIGURE 13. Simulation results of measured data, #1p, #2 and #3 (a) Change rate of runner speed (b) Head of casing inlet (c) Head of draft tube outlet.

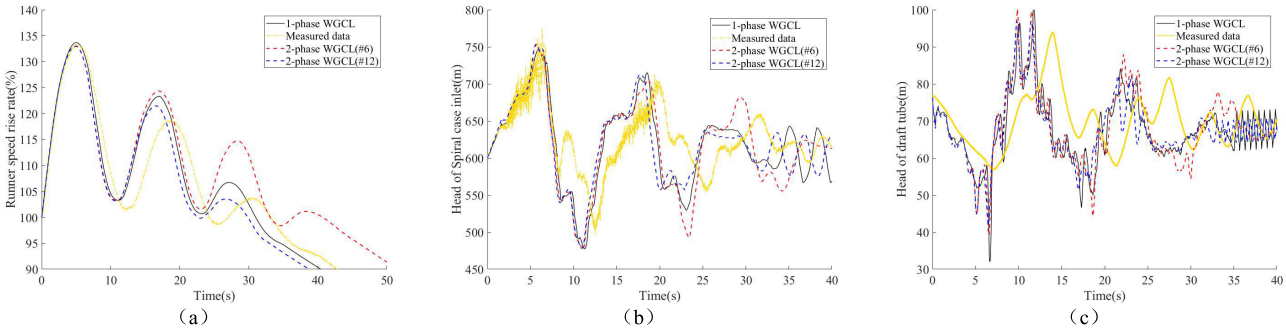

FIGURE 14. Simulation results of measured data, #1p, #6 and #12 (a) Change rate of runner speed (b) Head of casing inlet (c) Head of draft tube outlet.

If n performance indicators of Solution A outperform those of Solution B, then Solution A is nth-order non-dominated by B. For the two-phase WGCL, only Points 2 and 3 are entirely non-dominant for the two-phase WGCL Point 1p. Points 6, 7, 11, and 12 are second-order non-dominated by 1p, and other points are only first-order non-dominated by 1p. We select Points 2, 3, 6, and 12 for further analysis of its performance indicator curve.

As illustrated in Figs. 13 and 14, the fast-closing phase of the WGCL at Points 2 and 3 is very short, which can prevent the subsequent water hammer pressure from being too large for fast closing. However, the speed cannot be reduced significantly, and the overall closing curve is similar to a one-phase WGCL line. Points 6 and 12 have a longer period during the quick-closing phase, causing the rotation speed to drop, but it cannot suppress the subsequent increase in water hammer pressure.

The analysis results illustrate that the two-phase WGCL can reduce the extremum of related indicators to a certain extent, but the optimization range is limited. Especially for high-head pumped turbines, the highest water hammer often appears in the first phase. The extremum occurs earlier, resulting in insufficient time to reduce the speed through the quick shut-off. Next, we used the three-phase WGCL to compare the two-phase WGCL to analyze whether the relevant indicators can be further optimized.

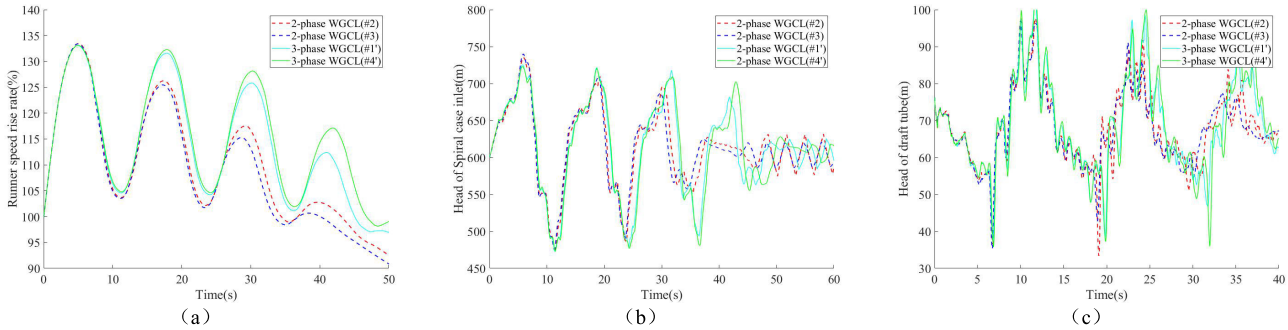

FIGURE 15. Simulation results of #2, #3, #1′ and #4′ (a) Change rate of runner speed (b) Head of casing inlet (c) Head of draft tube outlet.

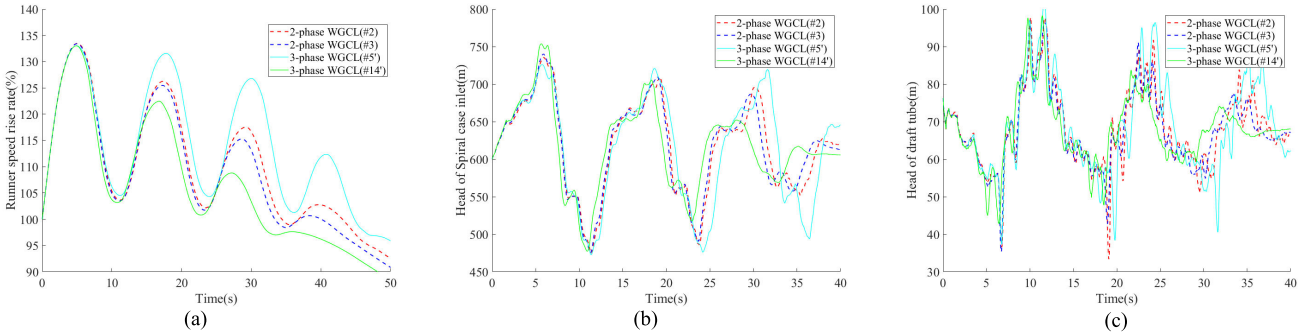

FIGURE 16. Simulation results of #2, #3, #5′ and #14′ (a) Change rate of runner speed (b) Head of casing inlet (c) Head of draft tube outlet.

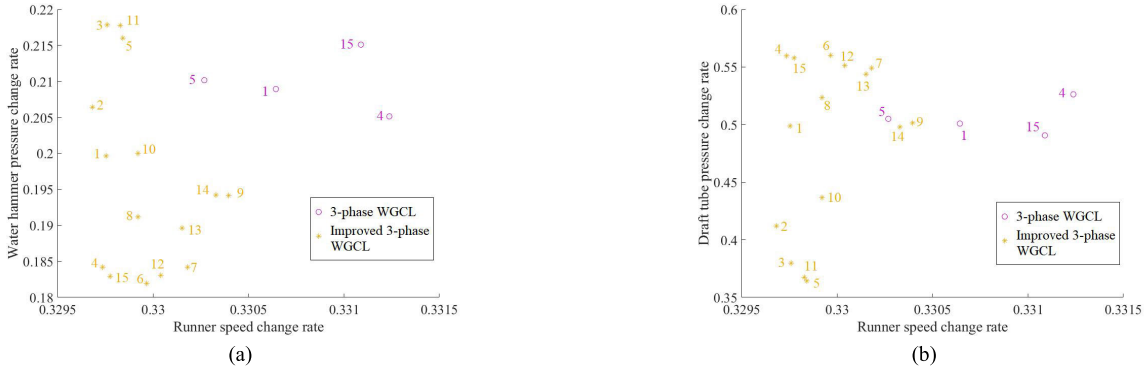

FIGURE 17. Elite solutions of 3-phase and improved WGCL (a) Change rate distribution of speed and water hammer pressure; (b) Change rate distribution of speed and draft tube pressure.

The points of the three-phase WGCL elite solution are followed by single quotation marks. Point 2 represents the solution in the two-phase closing law, and Point 2' represents the solution in the three-phase closing law. We use Points 2 and 3 as the optimal solution of the two-phase WGCLs. Based on Figs. 15 and 16, the two-phase WGCLs have been greatly improved, in which Point 1', 4', 5', and 15' are entirely non-dominated by Points 2 and 3.

Furthermore, although Points 8' and 14' are second-order non-dominated for Points 2 and 3, they are pronounced in reducing f_n and f_{H_2}. These two points represent the situation where the WGCL has a large negative pressure on the draft tube, a scenario that must be considered. Therefore, we select Points 1', 4', 5', and 14' for performance analysis.

The optimized three-phase WGCLs primarily adopt "close-close-close" mode. The four analysis points adopt the fastest closing method during the first phase of closing. For reducing the runner speed as much as possible, Points 1', 4', and 5' are closed in the second phase and maintain a large opening for a long period, effectively suppressing the water hammer of the first phase. Maintaining a relatively large opening for a long period will increase the subsequent fluctuations f_n and f_n, and the flow field will remain in a more severe state for a long period, which may intensify the influence of the blade channel vortex and the draft tube vortex strip.

Points 1', 4', and 5' become the fastest closing method again in the third section. At this time, the third-phase water

TABLE 8. 3-phase WGCL optimization scheme and performance parameters.

Elite solutions	t_1(s)	t_2(s)	t_3(s)	y_1(%)	y_2(%)	f_n	f_{H1}	f_{H2}
1	2.90	2.9	32.92	12.0	-9.8	0.3298	0.1997	0.4988
2	2.99	2.81	55.70	12.4	-10.0	0.3297	0.2064	0.4120
3	2.88	2.92	29.18	12.0	-10.0	0.3298	0.2178	0.3798
4	2.90	2.9	42.84	12.0	-10.0	0.3297	0.1842	0.5596
5	**2.84**	**2.96**	**29.85**	**11.8**	**-9.9**	**0.3298**	**0.2160**	**0.3645**
6	**2.78**	**3.02**	**39.89**	**11.5**	**-9.0**	**0.3300**	**0.1820**	**0.5603**
7	2.69	3.11	38.27	11.2	-9.3	0.3302	0.1842	0.5493
8	2.82	2.98	51.27	11.7	-8.1	0.3299	0.1912	0.5235
9	2.92	2.88	50.09	11.7	-9.3	0.3303	0.1941	0.5014
10	**2.95**	**2.85**	**55.61**	**12.2**	**-8.5**	**0.3299**	**0.2000**	**0.4368**
11	2.84	2.96	29.29	11.8	-9.9	0.3298	0.2177	0.3673
12	2.89	2.91	38.79	11.7	-9.8	0.3300	0.1831	0.5513
13	2.89	2.91	47.57	11.7	-9.5	0.3302	0.1897	0.5436
14	2.90	2.9	50.44	11.7	-9.2	0.3303	0.1942	0.4980
15	2.90	2.9	40.09	12.0	-9.8	0.3298	0.1829	0.5578

hammer is about to occur in the casing inlet pipe, and f_{H_1} has dropped. Therefore, the use of fast closing can suppress f_n and f_n and continues to fluctuate. For Point 14', in the second-phase closing process, a faster closing method is adopted, which suppresses subsequent speed fluctuations and draft tube pressure pulsations. The extremum of the first-phase water hammer pressure is then higher. The third phase adopts a slower closing method than the second phase, which can further absorb the pressure vibration caused by the subsequent water hammer, such that that f_{H_1} will stabilize as soon as possible.

It is evident from the typical solution that the optimized WGCLs adopt the fast-first-and-then-slow law (including the first two phases of the three-phase schemes), which demonstrates that this law is effective in reducing and balancing the three performance indicators. The two-phase WGCLs are limited by the short fast-closing time and the long slow-closing time, which is not suitable for the load rejection process in high-head PSPSs. For low-head power stations, the highest water hammer often appears in the last phase. There is a long period to close slowly, so it is more suitable to use two-phase WGCLs. The three-phase WGCLs reduces the amplitude of the second-phase closing and completely closes it in the third-phase, which can further reduce f_{H_1}. Based on analyzing the pressure curve results, the three-phase WGCLs are suitable for the load rejection process in high-head PSPSs.

B. COMPARISON OF IMPROVED 3-PHASE AND 3-PHASE WGCL

For the three-phase WGCLs, the wicket gates with a larger opening in the second stage can suppress the occurrence of the first-phase water hammer. The ''close-delay-close'' and ''close-reopen-close'' WGCLs are more conducive to the reduction in performance indicators [9], [17]. Simultaneously, the first turning point is generally selected at the extremum of the first-phase water hammer. Therefore, we improved the parameter settings of the algorithm, narrowed the parameter range of the optimization objectives, and performed a new round of optimization calculations. The obtained elite solution set is depicted in Table 8 and compared with the four completely non-dominated solutions of the three-phase WGCL in Fig. 17. The improved three-phase WGCLs elite solution is followed by double-quotes. 5'' represents an improved three-phase WGCL, and 5' represents a three-phase WGCL.

Compared with the four optimal solutions of the three-phase WGCL, most of the improved three-phase elite solutions are second-order non-dominated, and only the Point 10'' is completely non-dominated. In the optimized result, f_n was difficult to reduce further, but Points 5'' and 6'' reduce the values of f_{H_1} and f_{H_2}, respectively. We select Points 5'', 6'', and 10'' to compare with the three-phase Point 5', and the performance index curve is depicted in Fig. 18.

The ''close-reopen-close'' WGCLs are adopted in the optimization results of the improved three-phase model, which further decreases f_{H_1}. The WGCLs of Points 5,'' 6'' and 10'' are roughly equivalent in the first two phases, ith the primary difference being the law of the third-phase. The closing speed of Point 5'' is the fastest, and the flow rate decreases rapidly, such that it can prevent a low-pressure fluctuation at the draft tube. However, the pressure extremum of the second-phase water hammer is too large, even exceeding that of the first phase. The closing speed of Point 6'' is slow in the third phase, and a is suppressed in the second-phase water hammer, but a higher f_{H_2} appears in the second-phase. The average method is Point 10,'' and both f_{H_1} and f_{H_2} have achieved reasonable control, which is the ideal WGCL. Compared with the designed one-phase WGCL, the performance indicators of 10'' are reduced by 2.7%, 14.0%, and 17.5%, respectively.

C. OPERATING TRAJECTORY ANALYSIS OF WGCLS

We further analyzed the trajectory of WGCL working points with different schemes on the characteristic curve. The S-characteristics of the pumped turbine result in the unit parameters not converging as fast as for other conventional turbines. If the operating trajectory remains near the runaway curve for a long period during wicket gate closing, it is easy to cause small amplitude vibration, which is not conducive to the stability of the unit and may lead to more accidents.

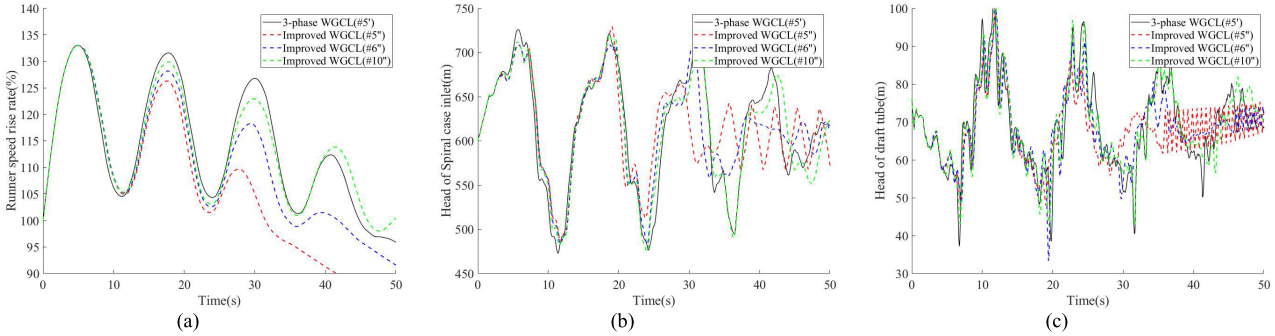

FIGURE 18. Simulation results of #5′, #5″, #6″ and #10″ (a) Change rate of runner speed (b) Head of casing inlet (c) Head of draft tube outlet.

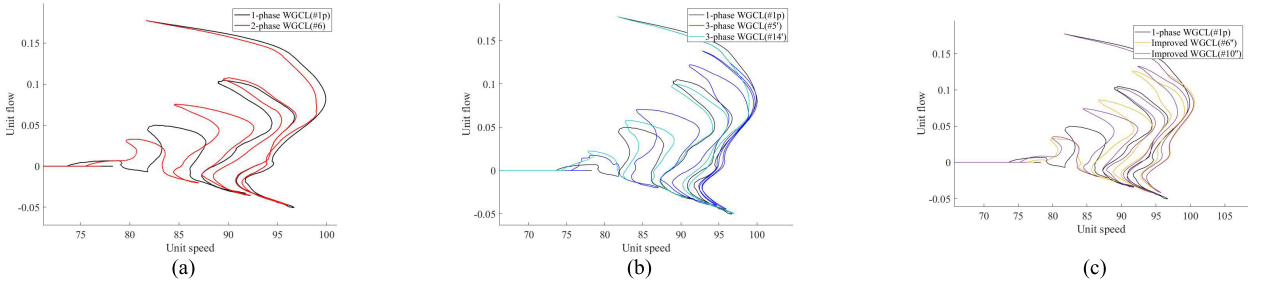

FIGURE 19. Operating trajectory of on the n_{11}-Q_{11} characteristic curve (a) #1p and #6 (b) #1p, #5′ and #14′ (c) #1p, #6″, #10″.

We selected Point 1p of the one-phase WGCL and Point 6 of the two-phase WGCL. Fig. 19(a) illustrates the changes in the trajectory of these two working points on the n_{11}-Q_{11} characteristic curve. After the load rejection condition occurs, the closing speed of Point 6 is faster than that of Point 1p, and it enters the slow phase at 4.23 s. At this time, the trajectory is close to the first singular point. It shifts the trajectory of Point 6 further to the left than that of Point 1p from the singular point, which increases the speed and enters the runaway region earlier.

When $Q_{11} = 0, f_{H_1}$ has an extremum, because the working point passes through the boundary of the reverse pump region earlier, the first-phase water hammer pressure becomes larger. In the subsequent slow-closing process at Point 6, when the working point gradually shifts to the right side of the Point 1p trajectory, the working point will experience a longer time in the runaway region. Simultaneously, when the second-phase water hammer comes, due to the large wicket gate opening and flow, the head rising effect caused by the water hammer cannot be reduced. Because the torque cannot be quickly reduced, the subsequent runner speed of the runner is also higher. Consequently, two-phase WGCLs cannot adapt to high-head PSPSs.

Fig. 19(b) illustrates the operating trajectories of the Point 1p of the one-phase WGCL and Points 5' and 14' of the three-phase WGCL on the characteristic curves. For three-phase WGCL, the initial quick closing causes the working point to move to the left, and the runner speed starts to decrease. Then, the second phase of slow closing causes the operating trajectory to move rapidly to the right, causing the working point to pass $Q_{11} = 0$ at a later time, effectively reducing the extremum of water hammer pressure. After the fast closing of the third phase, the trajectory is moved to the left again, which dramatically shortens the time for the follow-up work point in the runaway region.

Fig. 19(c) illustrates the trajectory of the Point 1p of the one-phase WGCL and Points 6'' and 10'' of the improved three-phase WGCL on the characteristic curves. For these schemes, the reopening operation of the second-phase makes the trajectory directly shift to the right of the Point 1p trajectory line, causing the time of the working point moving to line $Q_{11} = 0$ to increase, reducing the pressure extremum of the casing inlet. Simultaneously, the third phase is again closed quickly, reducing the time to move in the runaway region.

Based on the optimized results of NSGA-III, we believe that the WGCL corresponding to Point 10'' is the best way to solve performance indicator deterioration during the load rejection transient process. This scheme has achieved significant improvements in the three performance indicators of the increase in runner speed, water hammer pressure of the casing inlet, and pressure of the draft tube outlet. Under the 100% load rejection condition of high-head PSPSs, the use of the ''close-reopen-close'' three-phase WGCLs can prevent the occurrence of undesirable phenomena.

VI. CONCLUSION

Previous researchers rarely used MO optimization methods to study the WGCL problem of the high-head PSPS. The three key parameters that restrict each other—runner speed, casing inlet pressure, and draft tube outlet pressure—represent a

single-objective optimization problem. In this study, the operating characteristics of high-head PSPSs under load rejection conditions were explained, and the impact of three indicators on the equipment should be minimized. Combined with the NSGA-III algorithm, different WGCLs were studied, and a scheme of improved three-phase WGCL was proposed.

The main research results are as follows:

1) A 1D numerical model was established to accurately simulate the transient operation of a high-head PSPS, and explain how the wicket gate closing process affects the change law of different parameters under load rejection industrial control. The operating trajectories of the working point on the S-characteristic curves were analyzed quantitatively, and the changes in the internal flow field of the pumped turbine under load rejection conditions were researched using 3D-CFD.
2) The NSGA-III algorithm—suitable for calculating multiple objective functions and multiple constraints—was introduced, and its special selection algorithm was further elaborated. For the first time, NSGA-III was applied to calculate the MOWGCL problem for high-head PSPSs. Based on optimizing the WGCLs of a PSPS unit, the optimization algorithm is suitable for multi-objective engineering problems.
3) We analyzed the optimized WGCL, and compared the impact of one-phase, two-phase, and three-phase WGCLs on the changes in key parameters. Simultaneously, we comprehensively analyzed the possible impact of each key parameter on the unit equipment. A scheme of improved three-phase WGCL was proposed, and the specific closing schemes were precisely optimized through NSGA-III. By analyzing the working point's operating trajectory, a mechanism of WGCL to avoid the runaway region and pressure extremum was proposed.

The results of this study demonstrate the superiority of the heuristic MO optimization algorithm NSGA-III for solving real-world engineering problems. The optimization results and law analysis guided the control and safe operation of hydropower equipment. Few people have studied the influence of WGCLs on the 3D runner, future research will develop from 1D numerical models to 3D models.

NOMENCLATURE

a	slope of any point on operation trajectory
c	water hammer wave velocity
D	pipe diameter
D_1	inlet diameter of runner
f	hydraulic friction coefficient
F	area of the pipe section
g	gravity constant
h	dimensionless water head
H	water head
H_1	head of spiral case inlet
$H_{1,r}$	initial state of head of spiral case inlet
H_2	head of draft tube outlet
$H_{2,r}$	initial state of draft tube outlet
L	length of piezometric pipe
M_{11}	unit torque
M_{11}'	dimensionless unit torque
M_t	calculated torque of the MOC model
n	rotational speed of runner
N	number of total time node
n_r	initial state of speed
n_{11}	unit speed
n_{11}'	dimensionless unit speed
Q	flow
Q_{11}	unit flow
Q_{11}'	dimensionless unit flow
Q_t	calculated flow of the MOC model
t	time
T_a	time scales of machinery
T_w	time scales of water flow
α	wicket gate opening

REFERENCES

[1] S. Chen, J. Zhang, G. Li, and X. Yu, "Load rejection test and numerical prediction of critical load case scenarios for pumped storage plant," in *Proc. Sympo, Keynotes, Adv. Numer. Modeling Turbomachinery Flow Optimization, Fluid Machinery, Ind. Environ. Appl. Fluid Mechanics, Pumping Machinery*, Waikoloa, HI, USA, Jul. 2017, Art. no. V01AT03A009.

[2] G. Kahraman, "Investigation of the effect of operating conditions change on water hammer in hydroelectric power plants," *J. Failure Anal. Prevention*, vol. 20, no. 6, pp. 1987–1991, Dec. 2020, doi: 10.1007/s11668-020-01017-2.

[3] A. Bergant, A. R. Simpson, and A. S. Tijsseling, "Water hammer with column separation: A historical review," *J. Fluids Struct.*, vol. 22, no. 2, pp. 135–171, Feb. 2006.

[4] Z. Yao, H. Bi, Q. Huang, Z. Li, and Z. Wang, "Analysis on influence of guide vanes closure laws of pump-turbine on load rejection transient process," in *Proc. 6th ICPF*. Beijing, China: Tsinghua Univ, Sep. 2013, Art. no. 072004.

[5] C. Feng, L. Chang, C. Li, T. Ding, and Z. Mai, "Controller optimization approach using LSTM-based identification model for pumped-storage units," *IEEE Access*, vol. 7, pp. 32714–32727, 2019.

[6] J. Zhao, L. Wang, D. Liu, J. Wang, Y. Zhao, T. Liu, and H. Wang, "Dynamic model of kaplan turbine regulating system suitable for power system analysis," *Math. Problems Eng.*, vol. 2015, Nov. 2015, Art. no. 294523.

[7] X. Fu, D. Li, H. Wang, G. Zhang, Z. Li, and X. Wei, "Numerical simulation of the transient flow in a pump-turbine during load rejection process with special emphasis on hydraulic acoustic effect," *Renew. Energy*, vol. 155, pp. 1127–1138, Aug. 2020.

[8] B. Xu, D. Chen, S. Tolo, E. Patelli, and Y. Jiang, "Model validation and stochastic stability of a hydro-turbine governing system under hydraulic excitations," *Int. J. Electr. Power Energy Syst.*, vol. 95, pp. 156–165, Feb. 2018.

[9] W. Zeng, J. Yang, J. Hu, and J. Yang, "Guide-vane closing schemes for pump-turbines based on transient characteristics in S-shaped region," *J. Fluids Eng.*, vol. 138, no. 5, May 2016.

[10] M. Xiuli, P. Giorgio, and Z. Yuan, "Francis-type reversible turbine field investigation during fast closure of wicket gates," *J. Fluids Eng.*, vol. 140, no. 6, Jun. 2018.

[11] W. Wang, G. Pavesi, J. Pei, and S. Yuan, "Transient simulation on closure of wicket gates in a high-head francis-type reversible turbine operating in pump mode," *Renew. Energy*, vol. 145, pp. 1817–1830, Jan. 2020.

[12] H. Cui, H. Fan, and N. Chen, "Optimization of wicket-gate closing law considering different cases," in *Proc. 26th IAHR Symp. Hydraulic Machinery Syst.* Beijing, China: Tsinghua Univ, Aug. 2012, Art. no. 052008.

[13] J. Zhang, J. Hu, M. Hu, J. Fang, and N. Chen, "Study on the reversible pump-turbine closing law and field test," *Fluids Eng. Division Summer Meeting*, vol. 47519, pp. 931–936, Jan. 2006.

[14] A. E. Lyutov, D. V. Chirkov, V. A. Skorospelov, P. A. Turuk, and S. G. Cherny, "Coupled multipoint shape optimization of runner and draft tube of hydraulic turbines," *J. Fluids Eng.*, vol. 137, no. 11, Nov. 2015, Art. no. 111302.
[15] X. Peng, J. Zhou, C. Zhang, R. Li, Y. Xu, and D. Chen, "An intelligent optimization method for vortex-induced vibration reducing and performance improving in a large francis turbine," *Energies*, vol. 10, no. 11, p. 1901, Nov. 2017.
[16] A. Rezghi, A. Riasi, and P. Tazraei, "Multi-objective optimization of hydraulic transient condition in a pump-turbine hydropower considering the wicket-gates closing law and the surge tank position," *Renew. Energy*, vol. 148, pp. 478–491, Apr. 2020.
[17] X. Lai, C. Li, J. Zhou, and N. Zhang, "Multi-objective optimization of the closure law of guide vanes for pumped storage units," *Renew. Energy*, vol. 139, pp. 302–312, Aug. 2019.
[18] S. Chen, J. Zhang, and X. D. Yu, "Optimization of two-stage closure law of turbine wicket gates and its application," *Appl. Mech. Mater.*, vols. 249–250, pp. 636–641, Dec. 2012.
[19] K. K. Mandal and N. Chakraborty, "Short-term combined economic emission scheduling of hydrothermal systems with cascaded reservoirs using particle swarm optimization technique," *Appl. Soft Comput.*, vol. 11, no. 1, pp. 1295–1302, Jan. 2011.
[20] C. A. Coello Coello, "Evolutionary multi-objective optimization: Some current research trends and topics that remain to be explored," *Frontiers Comput. Sci. China*, vol. 3, no. 1, pp. 18–30, Mar. 2009.
[21] K. Deb and H. Jain, "An evolutionary many-objective optimization algorithm using Reference-Point-Based nondominated sorting approach, Part I: Solving problems with box constraints," *IEEE Trans. Evol. Comput.*, vol. 18, no. 4, pp. 577–601, Aug. 2014.
[22] H. Jain and K. Deb, "An evolutionary many-objective optimization algorithm using reference-point based nondominated sorting approach, Part II: Handling constraints and extending to an adaptive approach," *IEEE Trans. Evol. Comput.*, vol. 18, no. 4, pp. 602–622, Aug. 2014.
[23] K. Deb, A. Pratap, S. Agarwal, and T. Meyarivan, "A fast and elitist multiobjective genetic algorithm: NSGA-II," *IEEE Trans. Evol. Comput.*, vol. 6, no. 2, pp. 182–197, Apr. 2002, doi: 10.1109/4235.996017.
[24] X. Bi and C. Wang, "A reference point constrained dominance-based NSGA-III algorithm," *Control Decis.*, vol. 34, no. 2, pp. 369–376, Feb. 2019.
[25] Q. Liu, X. Liu, J. Wu, and Y. Li, "An improved NSGA-III algorithm using genetic K-Means clustering algorithm," *IEEE Access*, vol. 7, pp. 185239–185249, 2019.
[26] X. Bi and C. Wang, "A niche-elimination operation based NSGA-III algorithm for many-objective optimization," *Int. J. Speech Technol.*, vol. 48, no. 1, pp. 118–141, Jan. 2018.
[27] W. Mkaouer, M. Kessentini, A. Shaout, P. Koligheu, S. Bechikh, K. Deb, and A. Ouni, "Many-objective software remodularization using NSGA-III," *ACM Trans. Softw. Eng. Methodology*, vol. 24, no. 3, pp. 1–45, May 2015.
[28] Q. Liu, "Optimization of fire distribution for multiple SGSW based on improved NSGA-III," *Syst. Eng. Electron.*, vol. 42, no. 9, pp. 1995–2002, Sep. 2020.
[29] J.-H. Yi, S. Deb, J. Dong, A. H. Alavi, and G.-G. Wang, "An improved NSGA-III algorithm with adaptive mutation operator for big data optimization problems," *Future Gener. Comput. Syst.*, vol. 88, pp. 571–585, Nov. 2018.
[30] M. Zhang, "Analysis of closing law of guide vane of load rejection for ultra-high head reversible unit," *Water Resour. Power*, vol. 38, no. 5, pp. 139–143, May 2020.
[31] O. H. Souza, N. Barbieri, and A. H. M. Santos, "Study of hydraulic transients in hydropower plants through simulation of nonlinear model of penstock and hydraulic turbine model," *IEEE Trans. Power Syst.*, vol. 14, no. 4, pp. 1269–1272, Nov. 1999.
[32] P. Suter, "Representation of pump characteristics for calculation of water hammer," *Sulzer Tech. Rev.*, vol. 4, no. 66, pp. 45–48, 1966.
[33] X. B. Zheng, P. C. Guo, H. Z. Tong, and X. Luo, "Improved Suter-transformation for complete characteristic curves of pump-turbine," in *Proc. 26th IAHR Symp. Hydraulic Machinery Syst.* Beijing, China: Tsinghua Univ, Aug. 2012, pp. 19–23.
[34] Q. Qiang, "Analysis on delay closing law of guide vane of pumped storage units," *Hydropower Pumped Storage*, vol. 5, no. 6, pp. 93–98, Jun. 2019.
[35] N. Srinivas and K. Deb, "Multiobjective function optimization using non-dominated sorting genetic algorithms," *IEEE Trans. Evol. Comput.*, vol. 2, no. 3, Jun. 2000.
[36] D. Cavicchio, "Adaptive search using simulated evolution," Ph.D. dissertation, School Inf., Univ Michigan, Ann Arbor, MI, USA, 1970.
[37] Q. Lu, C. Liang, and E. Zhang, "A dynamic sharing scheme-based multimodal niche genetic algorithm," in *Proc. 7th World Congr. Intell. Control Autom.*, Jun. 2008, pp. 5333–5338.
[38] S. Shi, Y. Chen, and X. Yao, "NGA-inspired nanorobots-assisted detection of multifocal cancer," *IEEE Trans. Cybern.*, early access, Oct. 15, 2020, doi: 10.1109/TCYB.2020.3024868.
[39] I. Das and J. E. Dennis, "Normal-boundary intersection: A new method for generating the Pareto surface in nonlinear multicriteria optimization problems," *SIAM J. Optim.*, vol. 8, no. 3, pp. 631–657, Aug. 1998.
[40] Y. Tian, X. Xiang, X. Zhang, R. Cheng, and Y. Jin, "Sampling reference points on the Pareto fronts of benchmark multi-objective optimization problems," in *Proc. IEEE CEC*, Rio de Janeiro, Brazil, Jul. 2018, pp. 1–6.

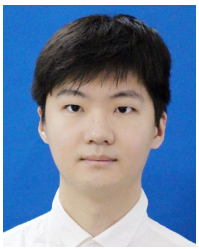

CHANG LIU received the B.S. degree in thermal energy and power engineering from the Central South University of Forestry and Technology, in 2016. He is currently pursuing the master's/Ph.D. degree with the School of Civil and Hydropower Engineering, Huazhong University of Science and Technology. His research interests include the influence of the transition process under the operating state of hydraulic machinery, and the strength analysis of equipment coupled with multi-physics.

JIANZHONG ZHOU is currently a Professor and the Doctoral Supervisor with the Huazhong University of Science and Technology, who is a major in the hydropower industry. He has published two monographs and published more than 300 articles in important academic journals, of which more than 100 articles have been included by SCI, EI, and ISTP. His research interests include advanced theories and methods of hydropower energy and its complex system analysis, power generation process control-diagnosis-simulation, and high-performance network and information systems.

XINJIE LAI received the B.S. degree in hydropower engineering from the Huazhong University of Science and Technology, in 2016, where he is currently pursuing the Ph.D. degree with the School of Civil and Hydropower Engineering. His research interests include the calculation of hydraulic transient process of hydro turbines and the optimization of control strategies of hydro turbine governing systems.

TIANYU ZHANG received the B.S. degree in energy and power engineering (hydrodynamic) from the North China University of Water Resources and Electric Power, in 2018. He is currently pursuing the Ph.D. degree in hydraulic engineering with the Huazhong University of Science and Technology. His research interests include the transition process and control of hydropower units.